Title
THE RATE OF THE RESONANT ENERGY-TRANSFER REACTION BETWEEN O2(1Ag) AND HOO

Authors
Podolske, J.R.
Johnston, H.S.

Publication Date
1982-07-01

LBL-14961
Preprint

Lawrence Berkeley Laboratory
UNIVERSITY OF CALIFORNIA

Materials & Molecular Research Division

Submitted to the Journal of Physical Chemistry

THE RATE OF THE RESONANT ENERGY-TRANSFER REACTION BETWEEN $O_2(^1\Delta_g)$ AND HOO

James R. Podolske and Harold S. Johnston

July 1982

Prepared for the U.S. Department of Energy under Contract DE-AC03-76SF00098

DISCLAIMER

LBL-14961
Preprint

Submitted to the Journal of Physical Chemistry

THE RATE OF THE RESONANT ENERGY-TRANSFER REACTION BETWEEN $O_2(^1\Delta_g)$ AND HOO

James R. Podolske and Harold S. Johnston

July 1982

Prepared for the U.S. Department of Energy under Contract DE-AC03-76SF00098

The Rate of the Resonant Energy-Transfer Reaction Between $O_2(^1\Delta_g)$ and HOO

James R. Podolske and Harold S. Johnston

Materials and Molecular Research Division, Lawrence Berkeley Laboratory

and Department of Chemistry, University of California,

Berkeley, California 94720

This work was supported by the Director, Office of Energy Research, Office of Basic Energy Sciences, Chemical Sciences Division of the U.S. Department of Energy under Contract Number DE-AC03-76SF00098.

Abstract

Photolysis of ozone at 253.7 nm in a flow system with helium carrier gas was performed, both without and with added water vapor, and steady-state ozone concentrations were measured by ultraviolet absorption at 315.0 nm. $O_2(^1\Delta_g)$ is a primary product of UV ozone photolysis, and in a pure ozone system each $O_2(^1\Delta)$ is responsible for the destruction of two additional ozone molecules. With water present, the $O(^1D)$ formed by O_3 photolyis reacts with H_2O to form hydroxyl radicals, and these radicals initiate an ozone-destroying chain reaction carried by HO and HOO radicals. The experimental results upon addition of water differed qualitatively from predictions based on the 1981 reaction set, but these differences could be explained in terms of inhibition of $O_2(^1\Delta)$ destruction of ozone by way of HOO quenching of $O_2(^1\Delta)$

$$HOO(^2A'') + O_2(^1\Delta_g) \rightarrow HOO(^2A', \nu_3 = 1) + O_2 \quad .$$

An experimental study under a variety of conditions and the interpretation of the data indicate this rate constant to be $3.3 \pm 1.6 \times 10^{-11}$ cm^3 $molecule^{-1}$ s^{-1}. The sensitivity of this result to the uncertainty in the rate constant for radical termination (HO + HOO) and vice versa was also investigated.

Introduction

The photolysis of ozone in the Hartley band has been shown to yield $O_2(^1\Delta_g)$ and $O(^1D_2)$ with a primary quantum yield of 0.9[1,2] and the other 0.1 is presumably $O_2(^3\Sigma_g^-)$ and $O(^3P)$. In a pure ozone system, further O_3 destruction occurs

$$O_3 + h\nu\ (253.7) \rightarrow O_2(^1\Delta) + O(^1D) \quad (1)$$

$$O(^1D) + O_3 \rightarrow O + 3/2\ O_2\ \text{(all channels)} \quad (2)$$

$$O_2(^1\Delta) + O_3 \rightarrow 2\ O_2 + O \quad (3)$$

$$2(O + O_3 \rightarrow 2\ O_2) \quad (4)$$

$$\text{net:}\quad 5\ O_3 + h\nu \rightarrow 7\ 1/2\ O_2 \quad . \quad (5)$$

Considering the 0.9 primary quantum yield for (1) and 0.1 quantum yield for $O_2 + O$, one expects an overall quantum yield of 4.7 from this mechanism. If O_2 and other buffer gas M are present, additional reactions need to be considered, which tend to lower the overall quantum yield

$$O(^1D) + M \rightarrow O + M \quad (6)$$

$$O_2(^1\Delta) + M \rightarrow O_2 + M \quad (7)$$

$$O + O_2 + M \rightarrow O_3 + M \quad . \quad (8)$$

When excess water is added to ozone undergoing photolysis, a chain reaction involving HO and HOO radicals is set up

INITIATION

$$O_3 + h\nu \rightarrow O_2(^1\Delta) + O(^1D) \quad (1)$$

$$O(^1D) + H_2O \rightarrow 2\ HO \quad (9)$$

CHAIN (OF LENGTH L)

$$HO + O_3 \rightarrow HOO + O_2 \quad (10)$$

$$HOO + O_3 \rightarrow HO + 2\ O_2 \quad (11)$$

TERMINATION

$$HO + HOO \rightarrow H_2O + O_2 \quad (12)$$

$$HOO + HOO \rightarrow H_2O_2 + O_2 \quad (13)$$

$$HO + H_2O_2 \rightarrow H_2O + HOO \quad (14)$$

SIDE REACTION

$$O_2(^1\Delta) + O_3 \rightarrow 2\ O_2 + O \quad (3)$$

$$O + O_3 \rightarrow 2\ O_2 \quad (4)$$

$$\text{net:}\quad (3 + 2\ L)\ O_3 + h\nu \rightarrow \text{oxygen} \quad (15)$$

A long chain length is favored by low radical concentrations, and low light intensities. When H_2O_2 reaches a steady state, the pair of reactions, (13) and (14), act as a termination step with the same net chemistry as reaction (12). The rate constants for reactions (1) - (4), (6) - (14) are regarded as fairly well known,[3] except for (12) and (13). The original goal of the experiment was to obtain additional information about the rates of (12) and (13).

This experiment was set up to measure the concentrations of HO, HOO, H_2O, and H_2O_2 by a tunable diode laser and to measure the concentration of O_3 by 315 nm absorption in a long-path system in which flowing ozone in helium was photolyzed alternately in the presence and absence of water. This program was modified when it was found that observations of

steady state O_3 did not agree with those predicted by a complete contemporary (1981) photochemical model of this system, which is abbreviated by the chain reaction above with (15) as net result. In order to explain the qualitative as well as quantitative features of the results, the nearly resonant energy-transfer reaction was added to the mechanism.

$$HOO(^2A'') + O_2(^1\Delta_g) \rightarrow HOO(^2A',\ \nu_3 = 1) + O_2(^3\Sigma_g^-) \qquad (16)$$

Evidence for the $^2A'$ first-excited state of HOO, predicted by Walsh,[4] has come from theoretical studies[5,6] and from emission[7-9] and absorption[10] studies. Investigation of the near infrared emission of HOO by Becker et al.[7] produced evidence that the $^2A' \rightarrow {}^2A''$ emission was being pumped by $O_2(^1\Delta)$, for which excitation to $^2A'(\nu_3 = 1)$ was energetically possible. This pumping mechanism was later used to probe for the presence of HOO in a flow tube by addition of metastable oxygen and observing the $^2A'(000) \rightarrow {}^2A''(000)$ emission at 1.43 μm.[11] Although it is stated[11] that the HOO - $O_2(^1\Delta)$ energy transfer is fast, no quantitative study of this exchange appears to have been published.

The HOO radical destroys ozone in the chain (10, 11), but through (16) it also destroys an ozone destroyer (3, 4). Under conditions of a short chain (10, 11) the addition of water to a photolyzed ozone flow causes the steady-state ozone to increase. The experiments reported here provide an estimate of the rate constant for reaction (16).

Experimental

A schematic diagram of the experimental apparatus is presented in Fig. 1. The reaction cell is a cylindrical quartz tube which has an

inside diameter of 15 cm and a length of 178 cm. The tube is closed at both ends by stainless-steel endcaps, which are mounted on a rigid steel frame and sealed onto the quartz tube with silicone rubber O-rings. Three 7.6 cm diameter mirrors with 1.85 m radius of curvature are mounted in the White configuration to give optical paths of 7.4, 14.8, 22.2, or 29.6 meter path length. The entrance and exit windows are calcium fluoride. The reaction cell and optical train are mounted on a Newport Research Corporation vibration-isolation table.

A kinematically mounted mirror at the front end of the optical train allows selection of any one of three spectroscopic light sources: (1) A Sylvania DE 450A deuterium arc lamp; (2) a six volt tungsten lamp for alignment; or (3) a Laser Analytic tunable diode laser. The diode laser system has a $Pb_{1-x}Cd_xS$ emitter of a composition to produce emission between 3395 - 3445 cm^{-1}. The emitter is cooled and thermostated by a Cryodyne Model 70 closed cycle helium refrigerator. Coarse tuning is attained by adjusting this temperature and fine tuning is done by varying the current through the diode. The diverging laser beam is made parallel by an f/1 ZnSe lens, and it goes through a four-position carousel optionally to insert a He-Ne alignment laser, a reference gas cell, or a 2.5 cm Ge etalon into the beam. The carousel is in the position labeled "etalon" in Fig. 1. The beam is focused and chopped by a Bulova 1800 Hz tuning-fork, passes through the long-path cell, and finally through a McPherson Model 2051 one-meter grating monochromator. The infrared beam was detected by a Santa Barbara Research Center indium antimonide photovoltaic detector operated at liquid nitrogen temperature., The ultraviolet beam used for ozone analysis was detected by an EMI 9783B photomultiplier tube.

The photolytic light for these experiments came from eight 30 watt General Electric G30T8 low pressure mercury germicidal lamps, which emit most of their output in the 253.7 nm Hg line. The cell was surrounded by high reflectance Alzak aluminum sheeting to increase light intensity and uniformity in the cell. Special constant-current circuits were built to control the intensity of these lamps. The light intensity outside the cell was measured by a UV enhanced silicon photodiode, and the light inside was measured by ozone or by hydrogen peroxide photolysis.

This experiment was controlled and data were recorded by a Digital Equipment Corporation PDP 8/E minicomputer having 32 K of memory. Data were stored on the dual drive Dectape unit, and a display scope allows real-time viewing of the data as they are collected. Data could be sent directly to the Lawrence Berkeley Laboratory (LBL) computer for detailed analysis and graphical display.

All gases used in this study were supplied by LBL. The carrier gas of extra pure helium flowed through a Matheson moisture and particulate filter and through a six to twelve mesh silica gel trap at liquid nitrogen temperature. Distilled water was stored in a glass saturator and vacuum degassed before use. Ozone was prepared from "high-dry" oxygen, which was purified by passage through a quartz tube containing copper turnings at 900 K and through a column of palladium on alumina pellets at 620 K, and through columns of ascarite and P_2O_5 on glass beads to remove CO_2 and H_2O. The purified oxygen went through an Ozone Research and Equipment Company ozonator and into a high capacity glass trap containing six to twelve mesh silica gel at 196 K to collect the ozone. The oxygen was driven off by a stream of helium.

In the steady state flow system there were four regions of uniform pressure with three locations of sharp pressure drop. The helium carrier gas first passed at 1.5 atmosphere pressure through a Manostate Predictability flowmeter, and the total flow rate was maintained at 3.38 STP liters min^{-1}. The carrier gas was then split into three parallel streams, each one with a Nupro stainless steel needle valve on the upstream end to drop the pressure (to about 130 Torr) and to regulate the carrier flow through the circuit. A mass flowmeter measured the flow of 0.26 STP liters min^{-1} through ozone trapped on silica gel at Dry Ice temperature, and a similar flowmeter measured the flow (0.74 or 0.074 STP liters min^{-1}) through a water saturator at 293.0 K. The pressure was not accurately measured at the water saturator, and thus it was necessary to measure the water concentration in the reaction cell rather than to calculate it from flow rates and vapor pressure. The three streams blended in a manifold before entering the reaction cell. The gases enter and exit the reaction cell through two identical, two-meter long disperser tubes running lengthwise along the top and bottom of the 15 cm diameter reaction cell. Considerable effort went into the design and construction of these disperser tubes so that they would give uniform emission along the two-meter length of the tube. They are 3/8 inch o.d. thin-wall Pyrex tubes with one cm long stainless steel capillary tubes (0.61 mm i.d.) protruding through the side every 8 cm. The pressure drop across each capillary was at least ten times the pressure drop along the full length of the disperser tube. The turbulence caused by the flow-in process kept the contents well mixed, so that the reaction cell acted as a stirred-flow reactor even though it is relatively long and narrow. The pressure dropped through the disperser tube to a uniform value of

67.5 Torr in the reaction cell, as measured by a Baratron gauge. The second disperser tube provided uniform exit of the gases along the length of the tube and into the evacuated manifold. The exit gases passed through a hot copper tube to destroy the ozone and then through the vacuum pump.

The ozone concentration was measured by optical absorption at 315 nm with the 1200 line mm^{-1} grating installed in the monochromator with 0.2 mm slits to give 0.167 nm resolution. The ozone spectrum was determined in this apparatus at 0.1 nm intervals between 310 and 320 nm, and the results (Table 1) agreed with published values.[12] The ozone concentration in the absence of photolysis was between 10 and 15 x 10^{15} molecules cm^{-3}.

The flow through water saturator could be rapidly bypassed, and the increase in pressure in the cell was 2.07 Torr at a flowrate of 0.74 STP liters min^{-1} through the saturator or 0.21 Torr at a flowrate of 0.074 STP liters min^{-1}. These pressure measurements gave a rough estimate of the water concentration in the cell, but accurate measurements were made by high resolution infrared absorption spectrometry. A water line at 3406.675 cm^{-1} has been well characterized;[13] the integrated line intensity is 6.90 x 10^{-23} cm^2 $molecule^{-1}$ cm^{-1}. The water line width (FWHM) was about 0.015 cm^{-1}, the width of the diode laser was about 10^{-3} cm^{-1}, and the diode laser was used to scan the water line at 3406.675 cm^{-1}, Fig. 2. The concentration of water was 6.8 x 10^{15} molecules cm^{-3} at the slow flowrate and 68 x 10^{15} molecules cm^{-3} at the flowrate of 0.74 STP liters min^{-1}.

Results

Ten experiments were carried out with five different photolysis-light intensities (2.5 - 15 x 10^{14} photons cm^{-2} s^{-1} as controlled by setting the current through mercury lamps) and with two water concentrations at each intensity (6.8 or 68 x 10^{15} molecules cm^{-3}). In each experiment measurements were made of I_o (the light intensity through the cell with only helium flowing), the concentration of ozone in the cell with photolysis lamps off, the steady-state concentration of dry ozone with the photolysis lamps on, the ozone concentration as a function of time when water was added to the flowing system, the ozone concentration as a function of time after the water was turned off, and finally the concentration of dry ozone in the dark.

The ozone concentrations as a function of time from just before addition of water (6.8 x 10^{15} molecules cm^{-3}) until about 300s later are presented for a high-intensity run in Fig. 3 and for a low-intensity run in Fig. 4. The concentration of ozone in the dark was about 12 x 10^{15} molecules cm^{-3} in each case, it was reduced to a steady-state value of about 8 x 10^{15} by the low light intensity and of about 4 x 10^{15} by the high light intensity. Addition of water caused a further reduction of ozone at low intensity (Fig. 4), but at high intensity the ozone concentration increased above its dry steady-state value upon addition of water (Fig. 3). (The dip at about 30 seconds was caused by transient disturbance to the flowing system as the water flow was switched on, and it does not have photochemical significance.) The model-calculated curves on Figs. 3 and 4 are discussed in a subsequent section.

The results of the ten runs are summarized in Table 2. At each of five lamp intensities, ozone concentrations are given for dark conditions and for the steady-state with dry photolysis, and the changes in the steady-state concentrations of ozone are given for low (6.8×10^{15}) or high (68×10^{15} molecules cm^{-3}) added water concentration. At high light intensities ozone increased upon addition of water. At low light intensities, which favors long chain lengths L in (15), the ozone concentration decreased upon addition of water.

Discussion

From Table 2 it can be seen that upon addition of water to photolyzed ozone, the steady-state concentration of ozone increased in most cases, for example Fig. 3. If one solves the complex mechanisms (5) and (15) by the usual steady-state algebraic methods using currently accepted values for the rate coefficients,[3] it is found that ozone decreases upon addition of water in all cases. The concentration of ozone as a function of time was calculated from an accurate numerical model (as described below) using the first 33 chemical reactions in Table 3, which are the complete set according to the 1981 chemical model.[3] The calculation included expressions for flow-in of O_3, O_2, H_2O, and He and for flow-out of all species in the system. This photochemical model unconditionally predicts a decrease in ozone in all cases; the observed increase in ozone is qualitatively inconsistent with the model. Thus observation indicates that the 1981 chemical model is incomplete in some sense, that is, some important species or reaction is not included. As noted in the introduction, the resonant energy-transfer reaction (16) between HOO and $O_2(^1\Delta_g)$ is known to be fast, although the rate constant is not

known. It can be seen qualitatively that (16) tends to remove reactions (3) and (4) from the mechanism of ozone photolysis in the presence of water (15). An approximate steady-state algebraic analysis shows the rate constant k_{16} to appear only in ratio to the constants k_{12} and k_{13}. So far as the ozone rate is concerned, one can mask the absence of (16) from the mechanism by an unduly large value of k_{12} or k_{13}. This interesting interpretation can be made without a detailed numerical study, but such a detailed analysis is required to reach quantitative conclusions. Reaction (16) was added to the first 33 in Table 3 in the model calculations.

Inspection of the ozone measurements made in the absence of photolysis showed that the flow rate of ozone from the saturator into the cell underwent a long-term drift. It initially increased, leveled off, and finally decreased with time. The initial increase is attributed to migration of adsorbed ozone in the silica gel trap toward the exit port, while the later decrease is due to depletion of ozone on the silica gel. These dark measurements of O_3 were fit to the functional form

$$[O_3] = C_1 e^{-\alpha_1 t} - C_2 e^{-(\alpha_1 + \alpha_2)t} \quad . \qquad (17)$$

The change of ozone with time is summarized in Table 4, and the agreement of the observations with the calculated function (17) is usually better than one percent. This function for the change of ozone with time during the experiments was used in the numerical modeling of this system.

The detailed numerical model used the 34 reactions of Table 3 and a model of flow-in and flow-out of the reaction cell. Because of the uniform injection and removal of gases from the dispersers along the full length of the cell, the flow model is that of a stirred-flow

reactor. The approximate value of the photolysis intensity $\underline{I}$ was known from the measured lamp current and from calibrations with static ozone decay or static H_2O_2 decay. This value was used in the model to calculate the steady-state ozone concentration under conditions of dry photolysis, and the nominal value of $\underline{I}$ was refined iteratively to give agreement between observed and calculated steady state dry ozone. The rate constants used were those of a 1981 NASA evaluation.[3] This evaluation regarded the rate constant k_{12} to be uncertain by a large factor and probably to fall in the interval 4 to 20 x 10^{-11} cm^3 $molecule^{-1}$ s^{-1}. These calculations were carried out using values for k_{12} between 2 and 32 x 10^{-11}. The calculations were made with a modified version of the CHEMK program,[14,15] based on Gear's method[16] for numerically integrating a system of differential equations, to obtain the concentration of all species as a function of time.

Figure 3 shows one set of observations and four model calculations for the situation after 6.8 x 10^{15} molecules cm^{-3} of water are added to a steady-state ozone situation in a dry cell. The three lower curves omit the energy-transfer reaction (16) between HOO and $O_2(^1\Delta_g)$, and the values of k_{12} are (from bottom up) 4, 8, and 16 x 10^{-11} cm^3 $molecules^{-1}$ s^{-1}. In all cases the calculated ozone decreased upon addition of water, whereas the observed ozone showed a substantial increase. The upper solid-line calculated curve in Fig. 4 is for the case of k_{12} = 8 x 10^{-11} and k_{16} = 3 x 10^{-11} cm^3 $molecule^{-1}$ s^{-1}. Aside from the initial perturbation caused by switching on the water flow, the calculated curve matches the observed curve both with respect to build-up as a function of time and the steady-state value. Calculated curves give an

equally good fit to the data for the following three pairs of rate coefficients (units of $10^{-11}/cm^3$ molecule^{-1} s^{-1})

k_{12}	k_{16}
4.0	4.4
8.0	3.0
16.0	2.4

The value one infers for k_{16} depends on the value one adopts for k_{12}; and conversely the smaller the value of k_{16} adopted, the larger is the value of k_{12} needed to fit the data. Figure 4 presents calculated and observed data at relatively low light intensity. The lower curve is for $k_{12} = 8 \times 10^{-11}$ and $k_{16} = 0$, and it falls far below the observed data. The upper calculated curve is for $k_{12} = 8 \times 10^{-11}$ and $k_{16} = 3 \times 10^{-11}$, the same pair as in Fig. 3, and again there is a satisfactory agreement between calculated and observed ozone.

Using the reaction set in Table 3, the entire experimental sequence (dark ozone, steady-state photolysis of dry ozone, steady-state photolysis of wet ozone, steady-state photolysis of dry ozone, and dark ozone) was simulated for the ten experimental conditions of Table 2, for values of $k_{12} = 2, 4, 8, 16$ and 32×10^{-11}, and for values of $k_{16} = 1, 2, 4, 8,$ and 16×10^{-11} cm^3 molecule^{-1} s^{-1}, so that 250 complete simultations were calculated. The simulation results for each experiment and each set of k_{12} and k_{16} values were averaged between 150 and 300 seconds (compare Figs. 3 and 4), which correspond to the flow-photolysis steady state. For each experiment I, the percent deviation PD(I), and percent root-mean-square deviation (PRD) between calculated and observed ozone were calculated by the formulas

$$PD(I) = 100 \left([O_3]_{CALC(I)} - [O_3]_{OBS(I)} \right) / [O_3]_{OBS(I)} \quad (18)$$

$$PRD = \left[(1/10) \sum_{I=1}^{10} PD(I)^2 \right]^{1/2} \quad (19)$$

The resulting 5 x 5 grid of PRD as a function of k_{12} and k_{16} was converted to a finer mesh grid (41 x 41) using bicubic spline interpolation. This second grid was used to produce a contour map of PRD as a function of k_{12} and k_{16} (Fig. 5). There is a range of correlated pairs of k_{12} and k_{16} that are equally capable of describing the experimental results, from about $k_{12} = 4 \times 10^{-11}$ with $k_{16} = 4 \times 10^{-11}$ to about $k_{12} = 20 \times 10^{-11}$ with $k_{16} = 1.8 \times 10^{-11}$ cm^3 $molecule^{-1}$ s^{-1}. For the values of k_{12} of 4, 8, and 16 x 10^{-11}, five closely spaced values of k_{16} as suggested by Fig. 5 were calculated for each of the ten runs and the PRD calculated as before. Cubic spline interpolation of the resulting curves of PRD versus k_{16} produced the following optimal values of k_{16} for each of the three values of k_{12} (units of 10^{-11})

k_{12}	k_{16}	PRD/%
4.0	4.4	2.02
8.0	3.0	1.47
16.0	2.4	1.44

Recent experimental values[17-22] indicate that the value of k_{12} is about 7 x 10^{-11}, which gives a best value of $k_{16} = 3.3 \times 10^{-11}$.

If O_2 and HOO are assumed to be hard spheres with diameters of 0.34 and 0.35 nm,[23] respectively, the calculated gas-kinetic rate constant

for this electronic energy-transfer reaction is 2.3×10^{-10} cm^3 $molecule^{-1}$ s^{-1}, and in this sense this process has a collision-efficiency of between 0.1 and 0.2. Comparison of the range of values obtained in this study with a list of $O_2(^1\Delta)$ quenching rate constants for other molecules[24] indicates that this energy-transfer process is about 10^7 times faster than quenching by a number of molecular species, presumably due to the near resonance between $O_2(^1\Delta_g \rightarrow {}^3\Sigma_g^-)$ and HOO $[^2A'(001) \rightarrow {}^2A''(000)]$.[7] Even the relatively fast reaction of O_3 with $O_2(^1\Delta)$ is 10^3 times slower than this process.

The fate of electronically excited perhydroxyl radical HOO* is not well characterized. The fluorescence rate has not been measured, but the fluorescence rate coefficient has been estimated theoretically[6] to be 132 s^{-1}. No rate constants for reaction with or deactivation by other molecules have been reported. The equilibrium constant K_{16} ($= k_{16}/k_{-16}$) for the energy transfer reaction gives some information

$$K_{16} = \frac{[O_2][HOO^*(v = 0)]}{[O_2(^1\Delta)][HOO(v = 0)]} \approx 3 \exp \varepsilon/kT \qquad (20)$$

about the reverse process where 3 is from the electronic multiplicity of O_2, the rotational partition functions for HOO and HOO* are assumed to be about the same, and ε is about 925 cm^{-1}, the energy difference in the zero vibrational state between reactants and products. If k_{16} is taken to be 3.3×10^{-11} cm^3 $molecules^{-1}$ s^{-1}, the value of k_{-16} is 1.2×10^{-13} at 298 K and 3×10^{-14} at 225 K. The rate coefficient for removal of HOO* by the reverse reaction is $k_{-16}[O_2]$, and this rate coefficient would equal the calculated[6] fluorescence rate if $[O_2] = 1 \times 10^{15}$ molecules cm^{-3} at 298 K or 4×10^{15} at 225 K. In this experiment the

concentration of ozone was 4 to 12 x 10^{15}, and the concentration of oxygen from the photochemical destruction of ozone was of about the same magnitude. The fact that this experiment detected a large effect outside the range of currently accepted reactions[3] indicates that collisional deactivation of HOO*

$$HOO(^2A') + M \rightarrow HOO(^2A'') + M \qquad (21)$$

has a rate constant substantially larger than 1.2 x 10^{-13} cm^3 $molecules^{-1}$ s^{-1}, the indicated value for k_{-16}.

The implications of this result should be examined in several contexts. Since HOO quenching of $O_2(^1\Delta)$ is so fast, its effects should be considered when analyzing the laboratory kinetics of O_x - HO_x systems. When ozone is being photolyzed below 300 nm to produce $O_2(^1\Delta)$, neglect of k_{16} may lead one to assign spuriously high values of k_{12} as illustrated by this experiment (Figs. 3, 4, 5). This source of systematic error in kinetic studies is reduced if a large concentration of oxygen is present (note the effect of reaction 8 following reaction 3). The following considerations are much more speculative. It may be noted that these reactions are exothermic:[25]

$$HO + HOO \rightarrow H_2O + O_2(^1\Delta) \qquad (22)$$

$$HOO + HOO \rightarrow H_2O_2 + O_2(^1\Delta) \qquad (23)$$

where HOO* denotes $HOO(^2A')$; the values of ΔH_o^o are respectively -188 and -46 kJ mol^{-1}. If reactions (22) and (23) occur, in a system containing HO and HOO, there would be production of $O_2(^1\Delta)$ and thus HOO*, and there might be unrecognized chemical reactions of HOO* in competition with its deactivation (21). Such reactions may explain some of the pressure effects[22] and discrepancies in the literature between reported values of k_{12} and k_{13}.

The magnitude of the effect of reaction (16) on stratospheric chemistry can be estimated. Recent measurements of HOO mixing ratio give 4.7×10^{-10} at 37 km.[26] At 37 km Krueger's 1976 U.S. Standard Atmosphere Mid-Latitude Ozone Model indicates an ozone mixing ratio at this altitude of 8.0×10^{-6}. The relative rates of destruction of $O_2(^1\Delta)$ at this altitude are:

Species, Q	k_Q	[Q]/[M]	Relative k_Q[Q]
Air	4.5×10^{-19}	1.0	1.00
O_3	4.4×10^{-15}	8.0×10^{-6}	0.08
HOO	3.3×10^{-11}	4.7×10^{-10}	0.03

Reaction (16) contributes a few percent to the quenching of $O_2(^1\Delta)$ in this region of the atmosphere.

In the upper stratosphere the mole fraction of $O_2(^1\Delta)$ is a few parts per million, and the ratio of $O_2(^1\Delta)$ to O_2 is about 10^{-5}. If reaction (16) is maintained at chemical equilibrium (20), then HOO* would be about one percent of HOO. Because of collisional quenching of HOO*, its photochemical steady state is probably less than the chemical equilibrium value, but even so some interesting excited-state chemistry of HOO* may occur in this region or some emission from HOO* might be detectable.

Acknowledgment

This work was supported by the Director, Office of Energy Research, Office of Basic Energy Sciences, Chemical Sciences Division of the U.S. Department of Energy under Contract Number DE-AC03-76SF00098.

References

1. R. K. Sparks, L. R. Carlson, K. Shobatake, M. L. Kowalczyk, and Y. T. Lee, J. Chem. Phys. 72, 140 (1980).
2. S. T. Amimoto, A. P. Force, J. R. Wiesenfeld, and R. H. Young, J. Chem. Phys. 73, 1244 (1980).
3. Chemical Kinetic and Photochemical Data for Use in Stratospheric Modelling, Evaluation No. 4, (NASA-Jet Propulsion Laboratory, Pasadena, California, January 1981).
4. A. D. Walsh, J. Chem. Soc. 2260 (1953).
5. J. C. Gole and E. F. Hayes, J. Phys. Chem. 57, 360 (1972).
6. S. K. Shih, S. D. Peyerimhoff, and R. J. Buenker, Chem. Phys. 28, 299 (1978).
7. K. H. Becker, E. H. Fink, P. Langen, and U. Schurath, J. Chem. Phys. 60, 4623 (1974).
8. K. H. Becker, E. H. Fink, A. Leiss, and U. Schurath, Chem. Phys. Lett. 54, 191 (1978).
9. R. P. Tuckett, P. A. Freedman, and W. J. Jones, Mol. Phys. 37, 379 (1979).
10. H. E. Hunziker and H. R. Wendt, J. Chem. Phys. 60, 4622 (1974).
11. I. Glaschick-Schimpf, A. Leiss, P. B. Monkhouse, U. Schurath, K. H. Becker, and E. H. Fink, Chem. Phys. Lett. 67, 318 (1979).
12. E. C. Y. Inn and Y. Tanaka, J. Opt. Soc. Am. 43, 870 (1953).
13. R. A. Toth, J. Quant. Spect. Radiat. Transfer 13, 1127 (1973).
14. G. Z. Whitten, Rate Constant Evaluation Using a New Computer Modeling Scheme, presented at the ACS National Meeting (Spring, 1974).

15. G. Z. Whitten and J. P. Meyer, CHEMK: A Computer Modeling Scheme for Chemical Kinetics (Systems Applications, Inc., San Raphael, California, 1979).

16. C. W. Gear, Numerical Initial Value Problems in Ordinary Differential Equations, (Prentice-Hall, New Jersey, 1971).

17. R.-R. Lii, R. A. Gorse, Jr., M. C. Sauer, Jr., and S. Gordon, J. Phys. Chem. 84, 819 (1980).

18. J. P. Burrows, R. A. Cox, and R. G. Derwent, J. Photochem. 16, 147 (1981).

19. U. C. Sridharan, L. X. Qiu, and F. Kaufman, J. Phys. Chem. 85, 3361 (1981).

20. L. F. Keyser, J. Phys. Chem. 85, 3667 (1981).

21. M. J. Kurylo, O. Klais, and A. H. Laufer, J. Phys. Chem. 85, 3674 (1981).

22. W. B. DeMore, J. Phys. Chem. 86, 121 (1982).

23. J. O. Hirschfelder, C. F. Curtiss, and R. B. Bird, Molecular Theory of Gases and Liquids (John Wiley and Sons, New York, 1954(, p 1111.

24. K. H. Becker, W. Groth, and U. Schurath, Chem. Phys. Lett. 8, 259 (1971).

25. D. L. Baulch, R. A. Cox, R. F. Hampson, Jr., J. A. Kerr, J. Troe, and R. T. Watson, J. Phys. Chem. Ref. Data 9, 466 (1980).

26. J. G. Anderson, H. J. Grassl, R. E. Shetter, and J. J. Margitan, Geophys. Res. Lett. 8, 280 (1981).

27. J. F. Noxon, Space Sci. Rev. 8, 92 (1968).

Table 1. Absorption cross sections (cm^2/molecule, base e) for ozone averaged over each Å.

λ(Å)	$10^{20}\sigma$	λ(Å)	$10^{20}\sigma$	λ(Å)	$10^{20}\sigma$
3100	10.31	3134	7.02	3168	3.97
3101	10.28	3135	7.06	3169	4.05
3102	10.26	3136	7.00	3170	4.13
3103	10.22	3137	6.86	3171	4.15
3104	10.10	3138	6.70	3172	4.09
3105	9.89	3139	6.55	3173	4.03
3106	9.70	3140	6.36	3174	4.00
3107	9.57	3141	6.20	3175	4.09
3108	9.51	3142	6.01	3176	4.24
3109	9.40	3143	5.78	3177	4.20
3110	9.37	3144	5.63	3178	4.05
3111	9.31	3145	5.49	3179	3.90
3112	9.26	3146	5.41	3180	3.77
3113	9.22	3147	5.36	3181	3.67
3114	9.21	3148	5.30	3182	3.55
3115	9.13	3149	5.27	3183	3.40
3116	8.94	3150	5.20	3184	3.24
3117	8.67	3151	5.12	3185	3.13
3118	8.38	3152	5.08	3186	3.06
3119	8.23	3153	5.14	3187	2.97
3120	8.06	3154	5.27	3188	2.91
3121	7.89	3155	5.43	3189	2.82
3122	7.77	3156	5.51	3190	2.75
3123	7.64	3157	5.43	3191	2.72
3124	7.51	3158	5.23	3192	2.77
3125	7.36	3159	5.04	3193	2.93
3126	7.21	3160	4.83	3194	3.09
3127	7.12	3161	4.67	3195	3.21
3128	7.04	3162	4.57	3196	3.17
3129	6.97	3163	4.47	3197	3.08
3130	6.91	3164	4.40	3198	3.02
3131	6.82	3165	4.26	3199	3.12
3132	6.85	3166	4.14	3200	3.22
3133	6.95	3167	4.04	3201	3.20

Table 2. The effect of adding water on the steady-state concentration of ozone under photolysis at 253.7 nm.

Photolysis Intensity 10^{14} photons cm^{-2} s^{-1}	$[O_3]/10^{15}$ molecules cm^{-3}		Change in $[O_3]/10^{15}$ upon added $[H_2O]/10^{15}$	
	Lamps off	Lamps on, dry	ΔH_2O 6.8	ΔH_2O 68
14.2	15.1	5.05	+0.29	+0.58
10.8	11.6	4.23	+0.30[a]	+0.48
7.68	9.9	4.30	+0.26	+0.39
4.78	13.8	8.15	-0.17[b]	-0.38
2.19	15.1	12.1	-0.61	-1.30

[a] Figure 3.

[b] Figure 4.

Table 3. Mechanism and rate coefficients used in simulation studies.

		$\sigma(cm^{-2}/molecule)$
$O_3 + h\nu$	$\rightarrow O_2(^1\Delta) + O(^1D)$	1.0E-17
$O_3 + h\nu$	$\rightarrow O_2 + O$	1.0E-18
$H_2O_2 + h\nu$	$\rightarrow OH + HO$	7.4E-20
		k^a
$O(^1D) + O_3$	$\rightarrow O_2 + O_2$	1.2E-10
$O(^1D) + O_3$	$\rightarrow O_2 + O + O$	2.3E-10
$O(^1D) + H_2O$	$\rightarrow OH + OH$	2.3E-10
$O(^1D) + O_2$	$\rightarrow O + O_2(^1\Sigma)$	3.6E-11
$O(^1D) + He$	$\rightarrow O + He$	1.0E-15
$O(^1D) + H_2O_2$	$\rightarrow OH + HO_2$	5.2E-10
$O_2(^1\Delta) + O_3$	$\rightarrow O_2 + O_2 + O$	4.4E-15
$O_2(^1\Delta) + H_2O$	$\rightarrow O_2 + H_2O$	4.0E-18
$O_2(^1\Delta) + O_2$	$\rightarrow O_2 + O_2$	1.7E-18
$O_2(^1\Delta) + He$	$\rightarrow O_2 + He$	8.0E-21
$O + O_3$	$\rightarrow O_2 + O_2$	8.8E-15
$O + O_2 + H_2O$	$\rightarrow O_3 + H_2O$	5.6E-33[b]
$O + O_2 + He$	$\rightarrow O_3 + He$	3.4E-34[b]
$O + O_2 + O_2$	$\rightarrow O_3 + O_2$	6.4E-34[b]
$O + O_2 + O_3$	$\rightarrow O_3 + O_3$	1.7E-33[b]
$O + OH$	$\rightarrow H + O_2$	4.0E-11
$O + HO_2$	$\rightarrow OH + O_2$	3.5E-11
$O + H_2O_2$	$\rightarrow OH + HO_2$	2.2E-15
$OH + O_3$	$\rightarrow HO_2 + O_2$	6.8E-14
$OH + OH$	$\rightarrow H_2O + O$	1.9E-12
$OH + OH + M$	$\rightarrow H_2O_2 + M$	2.6E-31[b]
$OH + H_2O_2$	$\rightarrow HO_2 + H_2O$	1.7E-12
$HO_2 + O_3$	$\rightarrow OH + O_2 + O_2$	1.6E-15
$HO_2 + HO_2$	$\rightarrow H_2O_2 + O_2$	3.6E-12
$H + O_3$	$\rightarrow OH + O_2$	2.9E-11
$H + O_2 + He$	$\rightarrow HO_2 + He$	1.8E-32[b]
$H + O_2 + H_2O$	$\rightarrow HO_2 + H_2O$	4.5E-31[b]
$H + O_2 + O_2$	$\rightarrow HO_2 + O_2$	5.6E-32[b]
$OH + HO_2$	$\rightarrow H_2O + O_2$	parameter
$O_2(^1\Delta) + HO_2$	$\rightarrow O_2 + HO_2$	parameter

[a] Units cm^3 $molecule^{-1}$ s^{-1} except as noted.

[b] Units cm^6 $molecule^{-2}$ s^{-1}.

Table 4. Changing ozone concentration with time in absence of photolyzing light; units of 10^{15} molecules cm^{-3}.

Time s	$[O_3]$ OBS.	$[O_3]$ CALC.	$\Delta[O_3]$ %
0	14.72	14.72	0.0
3390	15.64	15.64	0.0
6660	14.57	14.54	-0.2
9840	12.86	12.85	-0.1
10500	12.38	12.48	0.8
13740	10.81	10.69	-1.1
16920	9.04	9.08	0.4

Figure Captions

Figure 1. Schematic diagram of experimental apparatus.

Figure 2. Absorption profile measurements of the 3406.675 cm^{-1} H_2O transition. Trace A is the result of the first (broad) scan over the H_2O line. Trace B is the result of the second (narrow) scan over the H_2O line. (Note the separate baseline for the two scans.)

Figure 3. Calculated and observed changes in the steady-state concentration of photolyzed ozone as water is added to a dry system. The three lower curves are (from top down) k_{12} = 16, 8, 4 x 10^{-11} cm^3 $molecules^{-1}$ s^{-1} and $k_{16} = 0$; the upper calculated curve is for $k_{12} = 8 \times 10^{-11}$ and $k_{16} = 3 \times 10^{-11}$. High photolysis lamp intensity.

Figure 4. Similar to Figure 2. The lower curve is calculated with $k_{12} = 8 \times 10^{-11}$ and $k_{16} = 0$; the upper curve with $k_{12} = 8 \times 10^{-11}$ and $k_{16} = 3 \times 10^{-11}$. Low photolysis lamp intensity.

Figure 5. Contour map of percent rms deviation between calculated and observed steady-state ozone for ten experiments as a function of assumed values for rate constants k_{12} (HO + HOO) and k_{16} [HOO + $O_2(^1\Delta)$].

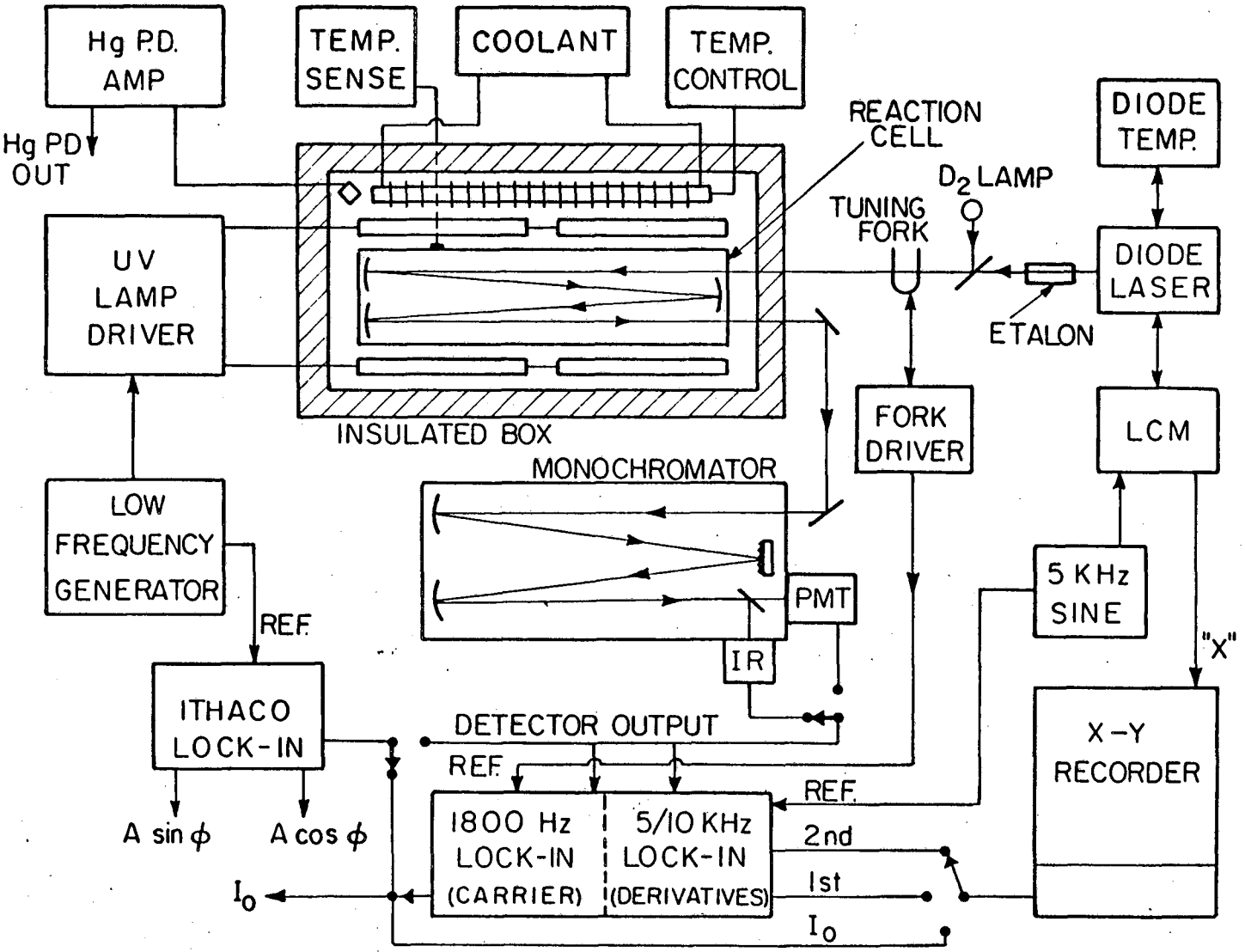

XBL 818-6378

Figure 1

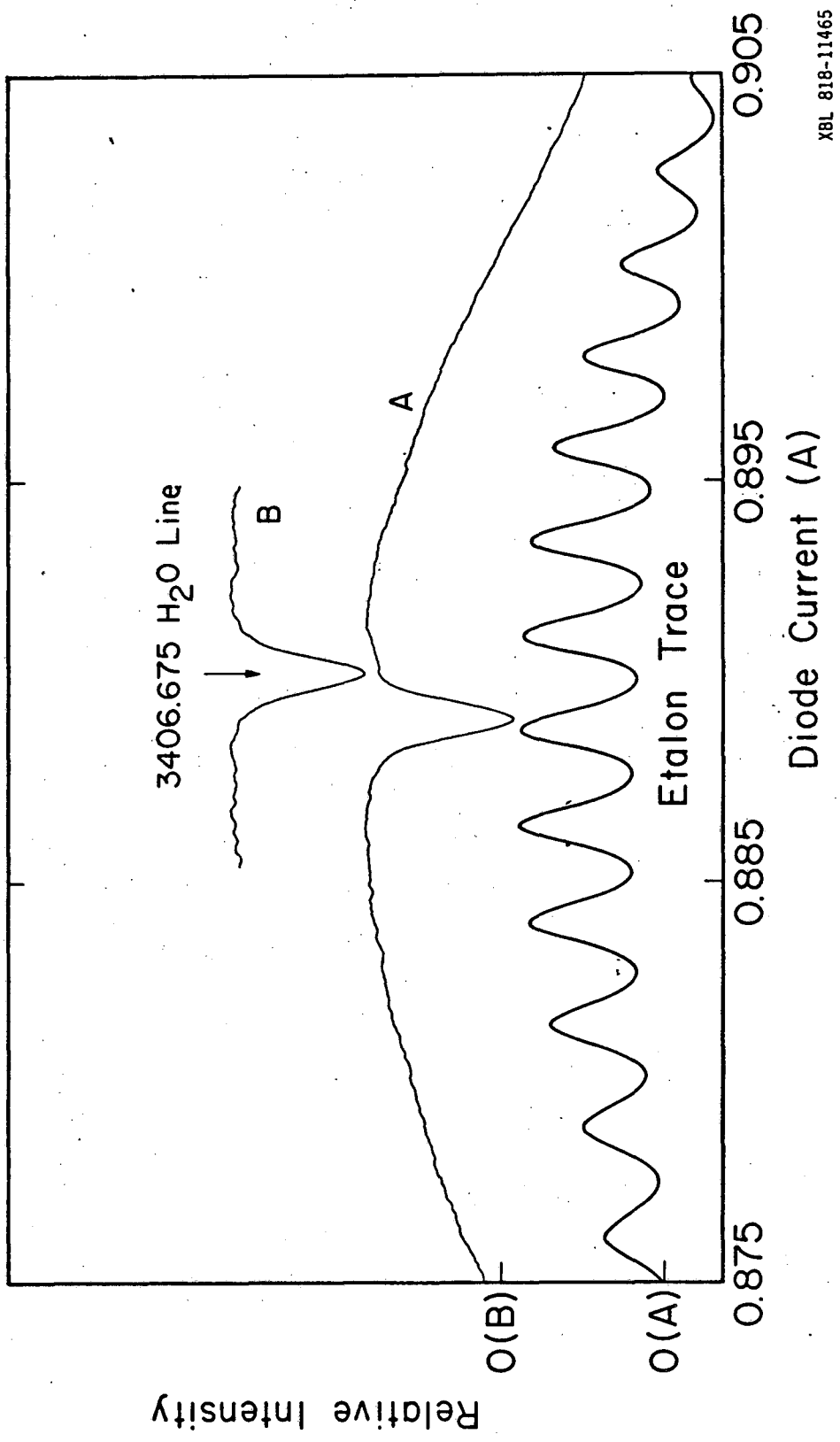
Relative Intensity
O(B)
O(A)
0.875
0.885
0.895
0.905
Diode Current (A)
Etalon Trace
3406.675 H_2O Line
B
A
XBL 818-11465

Figure 2

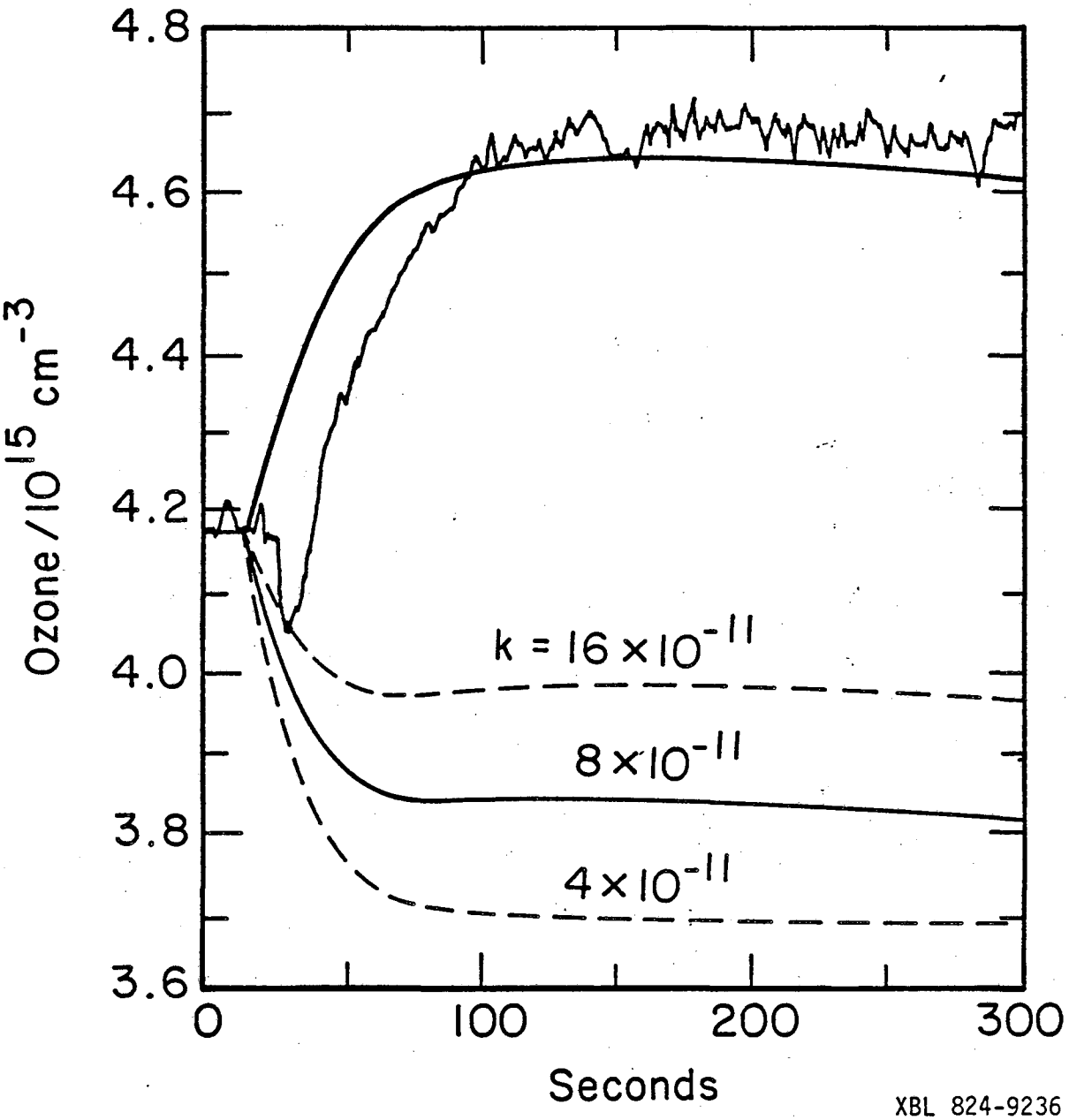
4.8
4.6
4.4
4.2
4.0
3.8
3.6
Ozone/10^{15} cm^{-3}
0
100
200
300
Seconds
k = 16×10^{-11}
8×10^{-11}
4×10^{-11}
XBL 824-9236

Figure 3

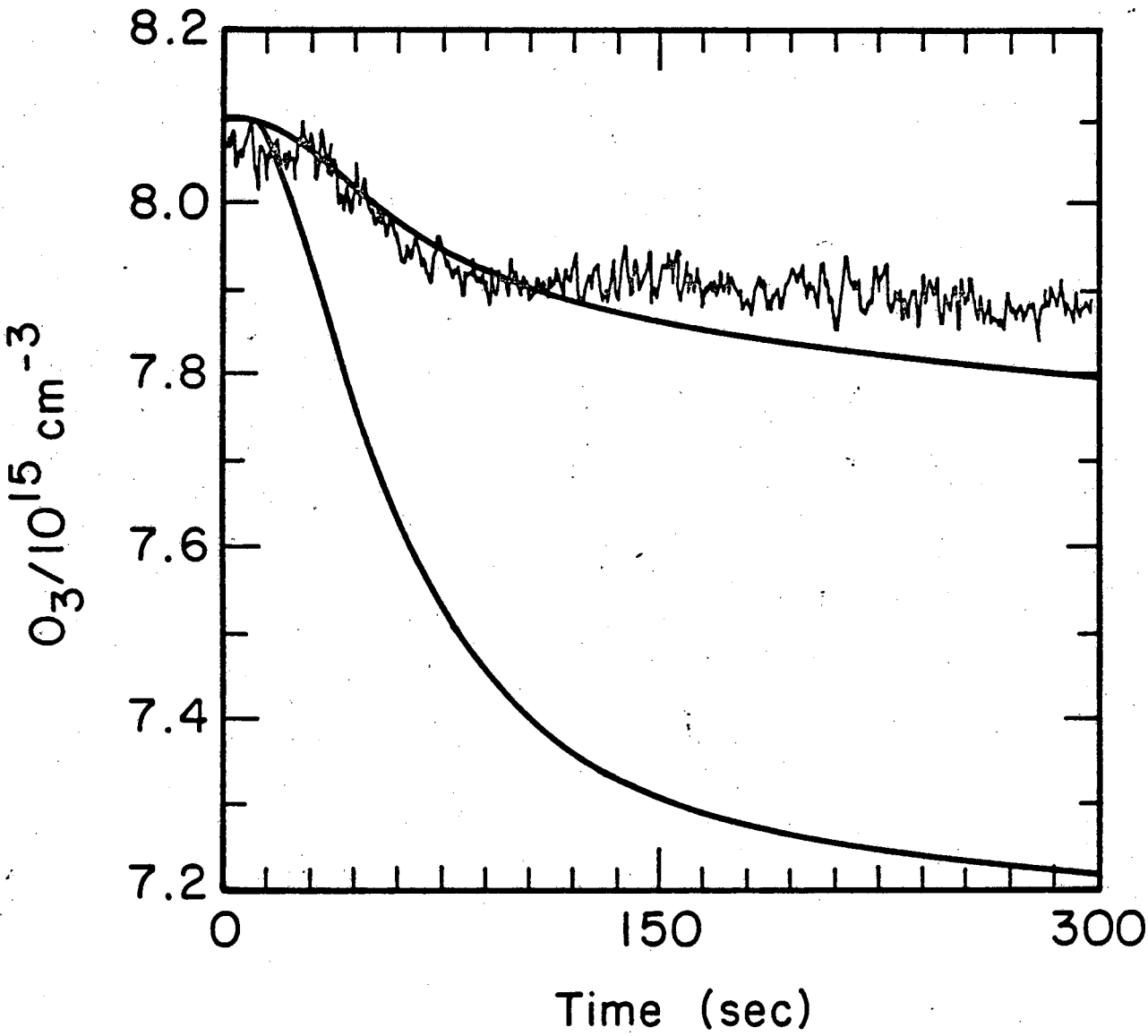

Figure 4

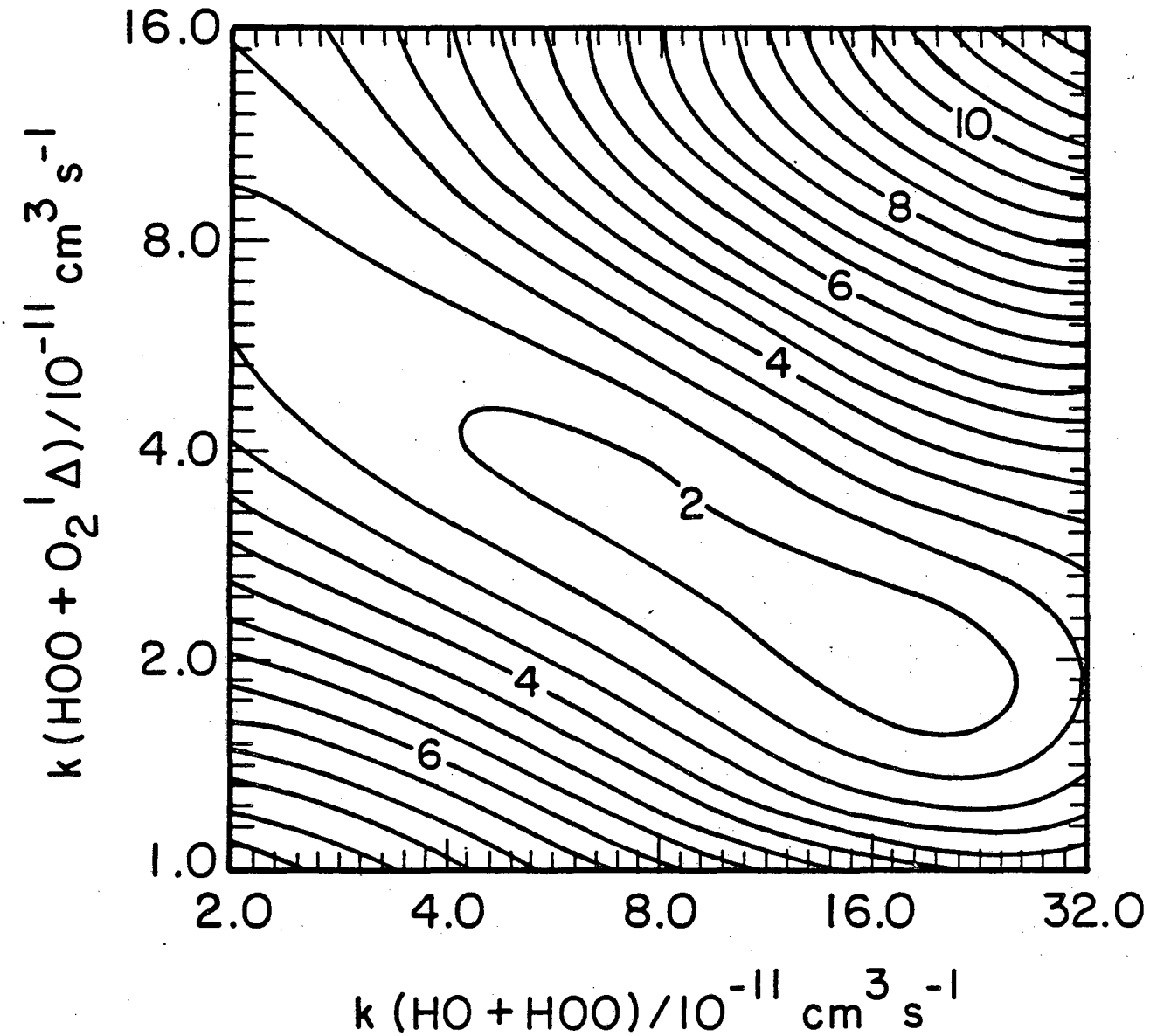
16.0
8.0
4.0
2.0
1.0
2.0
4.0
8.0
16.0
32.0
10
8
6
4
2
4
6
k(HOO + O2 1Δ)/10-11 cm3 s-1
k (HO + HOO)/10-11 cm3 s-1

Figure 5

TECHNICAL INFORMATION DEPARTMENT
LAWRENCE BERKELEY LABORATORY
UNIVERSITY OF CALIFORNIA
BERKELEY, CALIFORNIA 94720